Joule

CellPress

Article

# A Microporous and Naturally Nanostructured Thermoelectric Metal-Organic Framework with Ultralow Thermal Conductivity

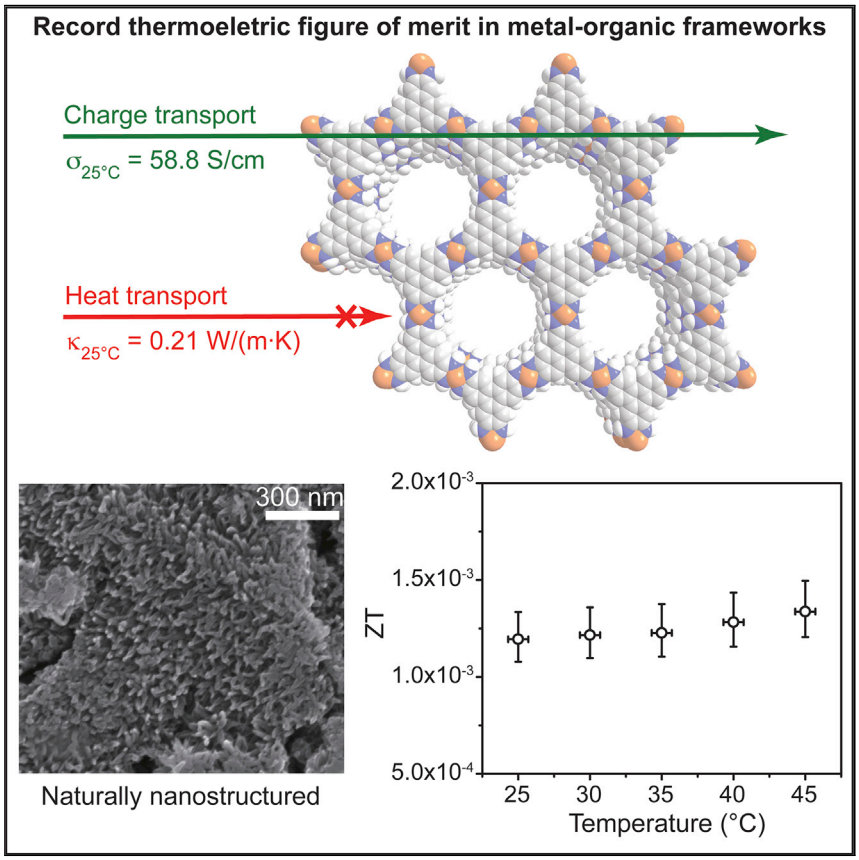


Thermoelectric devices utilize waste heat to generate electricity or consume electricity to transfer heat. Sun et al. describe high electrical conductivity and ultralow thermal conductivity in the nanoporous material $Ni_3(HITP)_2$, improve the record of thermoelectric figure of merit in metal-organic frameworks (MOFs), and demonstrate that MOFs are promising candidates for thermoelectrics.

Lei Sun, Bolin Liao, Dennis Sheberla, ..., Gang Chen, François Léonard, Mircea Dincă

mdinca@mit.edu

## HIGHLIGHTS

Thermoelectric characterization of a 2D MOF, $Ni_3(HITP)_2$

$Ni_3(HITP)_2$ consists of crystalline and naturally nanostructured particles

$Ni_3(HITP)_2$ exhibits ultralow thermal conductivity ($0.2\ W \cdot m^{-1} \cdot K^{-1}$) at 25°C

$Ni_3(HITP)_2$ displays record high thermoelectric figure of merit ($\sim 10^{-3}$) for MOFs

Sun et al., Joule 1, 168–177
September 6, 2017 
http://dx.doi.org/10.1016/j.joule.2017.07.018

Joule

CellPress

Article

# A Microporous and Naturally Nanostructured Thermoelectric Metal-Organic Framework with Ultralow Thermal Conductivity

Lei Sun,[1] Bolin Liao,[2] Dennis Sheberla,[1] Daniel Kraemer,[2] Jiawei Zhou,[2] Eric A. Stach,[3] Dmitri Zakharov,[3] Vitalie Stavila,[4] A. Alec Talin,[4] Yicong Ge,[1] Mark D. Allendorf,[4] Gang Chen,[2] François Léonard,[4] and Mircea Dincă[1,5,*]

## SUMMARY

**Microporous metal-organic frameworks (MOFs) offer attributes that make them potentially compelling choices for thermoelectric applications because they combine organic character with long-range order and intrinsically low thermal conductivity. So far, thermoelectricity in this class of materials has required infiltration with external molecules to render the framework electrically conductive. Here, we present thermoelectric studies on an n-type naturally nanostructured microporous MOF, $Ni_3$(2,3,6,7,10,11-hexaiminotriphenylene)$_2$, whose pressed pellets exhibit high electrical conductivity and low thermal conductivity. The results here show that by combining the structural rigidity and high crystallinity of inorganic materials, the solution-based synthesis of organic materials, and the unique pore-based tunability and low thermal conductivity, MOFs represent an intriguing new class of thermoelectric materials.**

## INTRODUCTION

Thermoelectric devices convert heat to electricity or vice versa, and are used to harness heat for power generation and for cooling applications.[1] The power conversion efficiency of a thermoelectric material scales with a dimensionless figure of merit $ZT = \frac{\sigma S^2 T}{\kappa}$, where σ is the electrical conductivity, S the Seebeck coefficient, κ the thermal conductivity, and T the absolute temperature.[1] Compelling enhancements in ZT have been achieved in recent years by exploiting nanostructuring and compositional engineering of inorganic materials,[2–4] as well as newly developed organic materials.[5] However, inorganic materials often require rare, environmentally unfriendly elements, while organic materials suffer from low charge mobility due to the absence of long-range order. New materials that facilitate electrical conduction and suppress thermal conduction are needed for high-performance thermoelectrics.

Introducing porosity into materials is a useful strategy to improve their thermoelectric performance because pores can strongly scatter phonons.[6] Importantly, porosity does not necessarily block charge transport. The continuous nonporous regions may still provide efficient charge transport pathways[7] because the electron and phonon wavelengths are different.[2] Therefore, porous solids could fit the requirements for an "electron-crystal phonon-glass," the ideal material for thermoelectrics.[2] An improved ZT is thus achievable when thermal conductivity is reduced to a larger extent than the power factor ($PF = \sigma S^2$). Indeed, a few inorganic solids with randomly distributed macropores (pore diameter >50 nm) and/or mesopores (pore diameter

### Context & Scale

Thermoelectric devices convert heat to electricity or vice versa. Their conversion efficiency scales with the thermoelectric figure of merit, ZT, which itself increases with increasing electrical conductivity and Seebeck coefficient, and with decreasing thermal conductivity. Owing to their monodisperse pores in the micro/mesoporous range, complex composition, and tunability, metal-organic frameworks (MOFs) offer promise in the context of thermoelectrics. Indeed, MOFs are excellent thermal insulators and recently have been shown to be good electrical conductors whose electrical conductivity and Seebeck coefficient may be optimized by design and/or post-synthetic tuning. Here, we present the thermoelectric properties of a naturally nanostructured MOF, $Ni_3(HITP)_2$, which exhibits an ultralow thermal conductivity and a record high ZT in this class of materials at room temperature. These intriguing properties reveal the potential of MOFs for high-performance thermoelectric applications.



CrossMark

between 2 and 50 nm) exhibit significantly reduced thermal conductivity and comparable ZT with the values of their nonporous parent materials.[8,9]

So far, little is known about the thermoelectric properties of periodic microporous materials mainly because it is technically challenging to generate such materials that exhibit significant electrical conductivity, especially by top-down methods such as lithography. In contrast, bottom-up, self-assembly strategies have generated a large number of microporous materials, among which metal-organic frameworks (MOFs) are representative. These materials are constructed by bridging metal ions with organic ligands, and usually exhibit high porosity and surface area as well as long-range translational symmetry.[10] The pores are periodically distributed and exhibit diameters typically ranging from 0.5 to 3 nm, which can be tuned both chemically and physically by choosing organic ligands of different composition and length. For instance, choosing long and flexible organic ligands could provide large pores and enhance phonon scattering.[11] Moreover, redox active metal ions and organic ligands could provide charge carriers.[7] The use of abundant and nontoxic metal elements could improve scalability and safety.

Recent advances in understanding thermal and electrical conduction in MOFs reveal promising thermoelectric properties. Although reports of thermal conductivity in these materials are limited, materials in this class investigated thus far all exhibit $\kappa < 0.4\ W \cdot m^{-1} \cdot K^{-1}$ regardless of structure, composition, or morphology,[12–18] with the single-crystal thermal conductivity of MOF-5 being as low as $0.32\ W \cdot m^{-1} \cdot K^{-1}$ at 27°C.[12] Despite their low thermal conductivity, MOFs have not been used extensively for thermoelectrics because they are typically electrical insulators. However, the last few years have seen significant advances in understanding and manipulating the electronic structure of these materials, with great improvements in electrical conductivity.[7,19–23] Indeed, there are now several MOFs[24] and structurally related coordination polymers[25–27] that exhibit room temperature $\sigma$ of $>1\ S \cdot cm^{-1}$. Even with low thermal conductivity, $\sigma$ values lower than $1\ S \cdot cm^{-1}$ typically greatly reduce ZT. This has been shown, for instance, with 7,7,8,8-tetracyanoquinodimethane-infiltrated $Cu_3$(benzene-1,3,5-tricarboxylate)$_2$ ($Cu_3(BTC)_2$-TCNQ), whose electrical conductivity of $7 \times 10^{-2}\ S \cdot cm^{-1}$ leads to a relatively low ZT of $7 \times 10^{-5}$ at 25°C, still a record for MOFs, despite a low $\kappa$ of $0.27\ W \cdot m^{-1} \cdot K^{-1}$ and high Seebeck coefficient of $375\ \mu V \cdot K^{-1}$.[18,20]

Clearly, improving the electrical conductivity should have a positive effect on ZT. To this end, the material $Ni_3$(2,3,6,7,10,11-hexaiminotriphenylene)$_2$ ($Ni_3(HITP)_2$) is an ideal case study.[24] It features a layered two-dimensional lattice consisting of $Ni^{2+}$ ions and $HITP^{3-}$ ligands arranged in a honeycomb structure. The layers are stacked, forming a graphite-like material with 1.5 nm-wide tubular pores running parallel to the *c* direction (Figure 1A). In agreement with the relatively big pore size, this material exhibits a high Brunauer-Emmett-Teller (BET) surface area of $630\ m^2 \cdot g^{-1}$.[28] More importantly, polycrystalline samples of $Ni_3(HITP)_2$ exhibit high $\sigma$ of approximately 50 $S \cdot cm^{-1}$, among the highest for polycrystalline MOFs.[24,29,30] Herein, we show that this high electrical conductivity leads to a 17-fold improvement of the ZT value compared with $Cu_3(BTC)_2$-TCNQ, representing a significant step forward in improving the thermoelectric performance of MOFs.

## RESULTS

Bulk $Ni_3(HITP)_2$ was synthesized according to a previously published procedure.[24] Its identity was confirmed by powder X-ray diffraction (PXRD; Figure S1) and its porosity was verified by $N_2$ sorption analysis, which revealed a BET surface area of

[1]Department of Chemistry, Massachusetts Institute of Technology, 77 Massachusetts Avenue, Cambridge, MA 02139, USA

[2]Department of Mechanical Engineering, Massachusetts Institute of Technology, 77 Massachusetts Avenue, Cambridge, MA 02139, USA

[3]Center for Functional Nanomaterials, Brookhaven National Laboratory, Upton, NY 11973, USA

[4]Sandia National Laboratories, Livermore, CA 94551, USA

[5]Lead Contact

*Correspondence: mdinca@mit.edu

http://dx.doi.org/10.1016/j.joule.2017.07.018

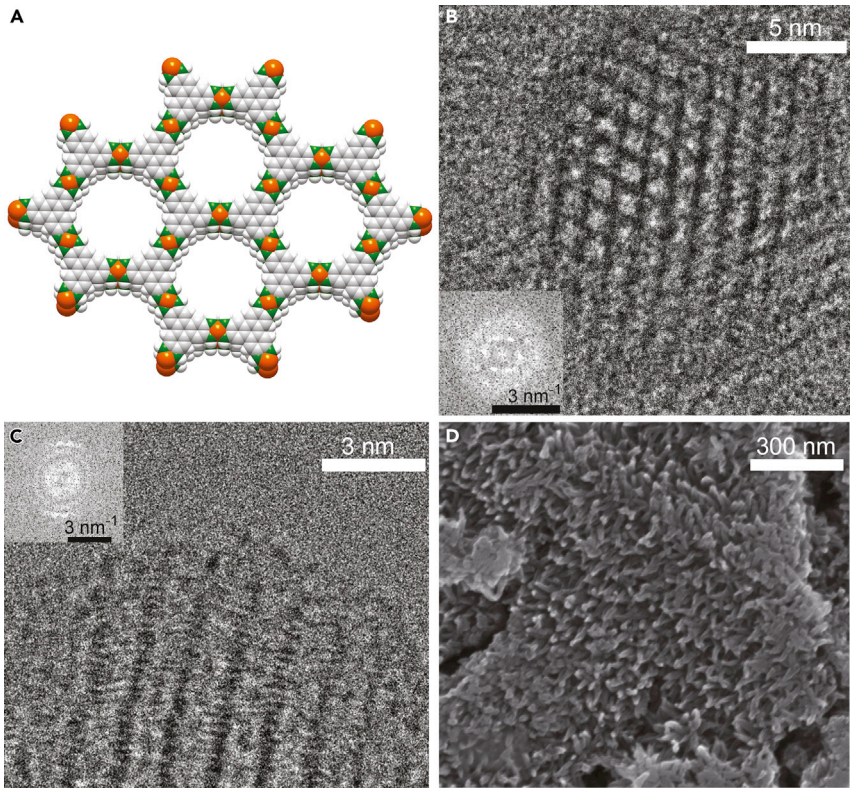


**Figure 1. Structure and Morphology of $Ni_3(HITP)_2$**

(A) A portion of the crystal structure of $Ni_3(HITP)_2$ showing multiple stacked 2D layers. Orange, green, gray, and white spheres represent Ni, N, C, and H atoms, respectively.

(B and C) TEM micrographs of $Ni_3(HITP)_2$ nanoparticles viewed along the pores (B) and perpendicular to the pores (C). Insets: FFT of the TEM images. See also Figure S3 and Table S1.

(D) Scanning electron micrograph of a $Ni_3(HITP)_2$ pellet showing complex morphology and grain boundaries. See also Figure S4.

766 $m^2 \cdot g^{-1}$ for the desolvated sample (for additional details see Experimental Procedures and Figure S2). Transmission electron microscopy (TEM) provided additional insight into the bulk structure of $Ni_3(HITP)_2$ by revealing two distinct morphological components: films and nanoparticles. The films likely form at the interface between the reaction mixture and air, as has been reported for related 2D MOFs.[25,30] The films appear extended, smooth, and folded in the TEM images, but do not diffract electrons, possibly because of electron beam damage (Figure S3A). Indeed, TEM imaging of MOFs is notoriously difficult: MOFs tend to decompose under a high-energy electron beam.[31–34] In contrast, the $Ni_3(HITP)_2$ nanoparticles appear crystalline (Figures S3B and S3C), with parallel 1D pores, 2D honeycomb lattices (Figure 1B), and stacks of multiple 2D sheets all clearly visible by TEM (Figure 1C). Fast Fourier transform (FFT) analysis from selected areas of the TEM micrographs, shown in Figures 1B, 1C, and S3D, revealed a hexagonal unit cell with cell parameters $a = b = 20.1$ Å, and $c = 6.6$ Å (Table S1). These are in agreement with the unit cell parameters obtained from the PXRD analysis and density functional theory calculations ($a = b = 21.8$ Å, $c = 6.7$ Å).[24] The interlayer stacking of $Ni_3(HITP)_2$ is irregular, and the corresponding FFT image displays arcs instead of spots for the (002) diffraction (Figure 1C inset), again in line with the broad peak at $2\theta = 27.3°$ in the PXRD pattern (Figure S1). Although the particle size varies widely, the largest $Ni_3(HITP)_2$ particles measure 20 × 20 × 50 nm, the latter dimension corresponding to approximately 150 stacked sheets.

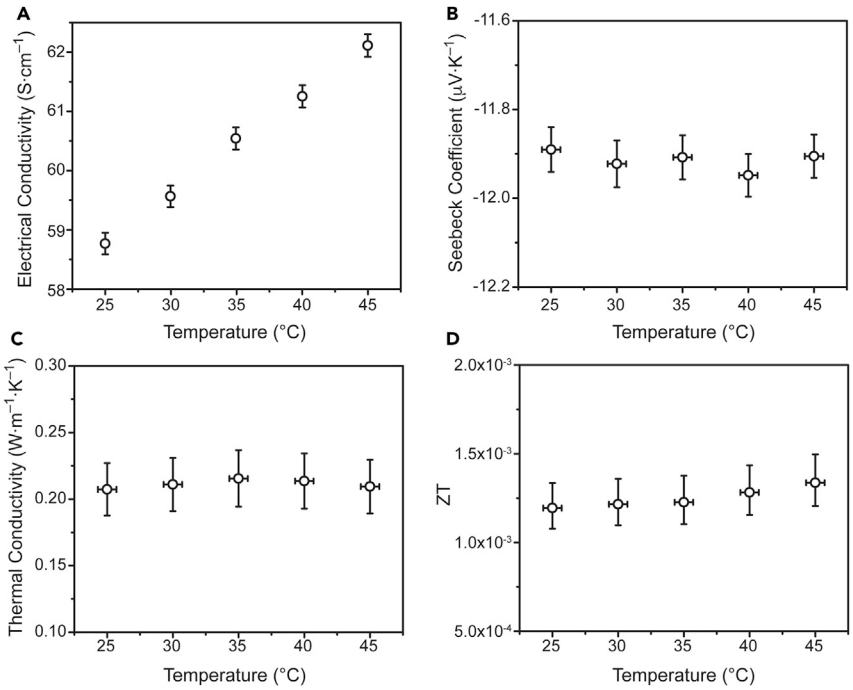


**Figure 2. Thermoelectric Properties of $Ni_3(HITP)_2$**

(A–D) Variable temperature electrical conductivity (A), Seebeck coefficient (B), thermal conductivity (C), and thermoelectric figure of merit (D). The error bars of electrical conductivity represent the combined error of both sheet electrical conductance and thickness measurements; the error bars of Seebeck coefficient and thermal conductivity represent standard deviation of multiple sweeps of the input heat power; the error bars of ZT represent the combined error of electrical conductivity, Seebeck coefficient, and thermal conductivity.

Pressed pellets of $Ni_3(HITP)_2$ were prepared by pressing powder samples under 1 GPa at room temperature for 15 min with a uniaxial hydraulic press. The pellets are circular plates with a diameter of 6 mm and thickness ranging from 300 μm to 2 mm. The PXRD pattern of the pressed pellets matched that of the powder (Figure S1), indicating that $Ni_3(HITP)_2$ retains its structure after pressure treatment at 1 GPa. The density of the as-prepared pressed pellets was approximately 1.0 g·cm$^{-3}$, slightly smaller than the crystallographic density (1.15 g·cm$^{-3}$) calculated from the precise formula of $Ni_3(HITP)_2$: $Ni_3(HITP)_{1.8}Cl_{0.6}\cdot 2(acetone)\cdot 4H_2O$ (see Experimental Procedures). This indicates the existence of grain boundaries and/or voids in the pressed pellets, as also verified by scanning electron microscopy (Figures 1D and S4). The nanoparticles were randomly oriented in the pressed pellets, such that the thermoelectric properties likely reflect averages of the intralayer and interlayer components. All thermoelectric characterizations were carried out between 25°C and 45°C. The electrical conductivity of the pellets was measured by the van der Pauw method.[35,36] The Seebeck coefficient and thermal conductivity were measured by the steady-state method using a home-built system that reaches high accuracy.[37–39] All thermoelectric properties were measured in vacuum ($10^{-5}$ to $10^{-4}$ torr) with the pressed pellets desolvated at 150°C for 2 hr.

As shown in Figure 2A, the electrical conductivity increased linearly with temperature from 58.8 S·cm$^{-1}$ at 25°C to 62.1 S·cm$^{-1}$ at 45°C. The pellets exhibited a negative room temperature Seebeck coefficient, S = −11.9 μV·K$^{-1}$, as shown in Figure 2B, indicative of n-type thermoelectric behavior.[40] S is nearly constant over this temperature range and defines a power factor ranging from 8.31 × $10^{-3}$ μW·cm$^{-1}$·K$^{-2}$ at

25°C to 8.80 × $10^{-3}$ μW·cm$^{-1}$·K$^{-2}$ at 45°C (Figure S5). These values are at least one order of magnitude higher than those observed for $Cu_3(BTC)_2$-TCNQ.[18] Importantly, the pressed pellets of $Ni_3(HITP)_2$ exhibited very low thermal conductivity, κ = 0.21 W·m$^{-1}$·K$^{-1}$ (Figure 2C). This value is much lower than those of conventional solid-state thermoelectric materials such as nanostructured $Bi_xSb_{2-x}Te_3$ ($\kappa_{pellet} \approx 1$ W·m$^{-1}$·K$^{-1}$ at room temperature)[41] and is comparable with the smallest values achieved for any thermoelectric materials.[5,42] As with S, κ is relatively constant over 25°–45°C.

With the relevant values of σ, κ, and S, pellets of $Ni_3(HITP)_2$ exhibit a ZT of 1.19 × $10^{-3}$ at 25°C, which increases to 1.34 × $10^{-3}$ at 45°C (Figure 2D). These values are approximately 17 times higher than those observed for $Cu_3(BTC)_2$-TCNQ, the previous record for MOFs, and are directly attributable to the higher electrical conductivity of $Ni_3(HITP)_2$.[18] Although this thermoelectric figure-of-merit value is still much lower than those required for practical applications (ZT > 1), it represents a new benchmark for ZT values in MOFs.

## DISCUSSION

The most prominent feature of $Ni_3(HITP)_2$ is its ultralow thermal conductivity, among the lowest for any crystalline solid-state material. In solids near room temperature, thermal conductivity can be divided into electronic ($\kappa_e$) and lattice ($\kappa_L$) contributions. The former is typically related to the electrical conductivity via the Wiedemann-Franz law, $\kappa_e = L\sigma T$, where the Lorenz number L is usually taken to be 2.44 × $10^{-8}$ W·Ω·K$^{-2}$.[43] For $Ni_3(HITP)_2$, whose electrical conductivity at 25°C is 58.8 S·cm$^{-1}$, $\kappa_e$ is 4.28 × $10^{-3}$ W·m$^{-1}$·K$^{-1}$. This value is much smaller than the experimentally observed bulk thermal conductivity in $Ni_3(HITP)_2$, 0.21 W·m$^{-1}$·K$^{-1}$, suggesting that $\kappa_L$ dominates the overall thermal transport in our material.

Several factors may contribute to the low lattice thermal conductivity of $Ni_3(HITP)_2$. First, phonons describe lattice vibrations that carry thermal energy, which cannot propagate across the intrinsic vacant pores. Second, the heterogeneity of atomic masses and stiffness of bonds in $Ni_3(HITP)_2$ cause phonon scattering. Third, the disordered stacking of the individual $Ni_3(HITP)_2$ layers, observed by TEM (Figure 1C), may cause additional phonon scattering. Finally, given the very small particle size of the crystallites within the $Ni_3(HITP)_2$ pellets, grain boundaries play an important role in scattering phonons as well. Indeed, nanostructuring, or breaking large crystallites into nanoparticles, is a widely used strategy to reduce $\kappa_L$ in thermoelectric materials.[44,45] However, generating nanostructured inorganic materials from bulk solids is challenging and energy consuming.[2] In this aspect, $Ni_3(HITP)_2$ is advantageous because it is naturally nanostructured.

Among the factors described above, the first two are likely general for all microporous/mesoporous MOFs, whereas the last two are specific for $Ni_3(HITP)_2$ pellets. Although the inaccessibility to large single crystals of $Ni_3(HITP)_2$ makes measuring its intrinsic thermal conductivity impractical, literature precedent for MOFs suggests that intrinsic factors are likely to dominate here too: as mentioned above, previously reported thermal conductivity values in MOFs are all smaller than 0.4 W·m·K$^{-1}$ at room temperature,[12–18] with single-crystal values reaching 0.32 W·m·K$^{-1}$ (in MOF-5).[12] Indeed, MOFs with high porosity and complex composition are all likely to behave as thermal insulators, such that improving the electrical conductivity and the Seebeck coefficient should lead to high-performance thermoelectrics. Although certain principles for achieving high

electrical conductivity in MOFs are now emerging,[7] improvements in Seebeck coefficient require fine-tuning of the band structure, a widely understudied concept in this class of materials.

In summary, $Ni_3(HITP)_2$ is the first example of an n-type thermoelectric MOF and exhibits a record thermoelectric figure of merit for this class of materials, approximately $10^{-3}$. The ZT of $Ni_3(HITP)_2$ is mainly limited by the small absolute value of its Seebeck coefficient, itself the result of the possible metallic nature of $Ni_3(HITP)_2$, suggested theoretically by its band structure.[46] Improvements in thermopower could be achieved by controlling the chemical doping or through further optimization of the hierarchical structure. Indeed, our tentative measurements on thin films of $Ni_3(HITP)_2$ have revealed a Seebeck coefficient of approximately $-50\ \mu V \cdot K^{-1}$ at 25°C, further confirming its n-type behavior, and highlighting the possibility to improve and tailor the thermoelectric properties through further processing.

Although these results describe a significant improvement in the ZT of MOFs specifically, the relatively low value in the context of the wider thermoelectrics field highlights the crucial need for additional systematic studies to further improve the thermoelectric performance of MOFs to meet the practical requirements. First, it is critical to achieve a high Seebeck coefficient because S influences ZT more significantly than other parameters ($ZT \propto S^2$). In this context, it would be initially productive to measure and tabulate the Seebeck coefficients of previously reported electrically conductive MOFs. This would enable a correlation between electrical conductivity and Seebeck coefficient in this class of materials. We also note that for traditional thermoelectric materials, the systematic variation of charge density serves as an important tool for optimizing the power factor. Here we have not optimized the charge density, but MOFs in general offer the opportunity for fine-tuning of this parameter and therefore of the power factor, especially when redox active. Second, as we have noted elsewhere,[7] there is a critical need for fundamental studies on the mechanism of charge transport in MOFs based on accurate measurements of charge mobility and charge density. Third, although these results point to an ultralow thermal conductivity as a potentially general feature of MOFs stemming from their periodic, porous, and compositionally complex structures, it is of increasing interest to investigate the influence of metal ions, pore size, structural rigidity, and the adsorbed guest molecules on thermal conductivity. Fourth, computational studies on the electronic band structure and phonon dispersion relation of microporous materials are helpful for understanding and optimizing their thermoelectric properties. Materials with large density of states near the Fermi level are especially attractive because they tend to exhibit large Seebeck coefficients. Finally, the applicability of current thermoelectric characterization methods to MOFs should be verified, and new characterization methods may be needed specifically for this class of materials. Beyond the exploration of MOFs as promising thermoelectric materials, these continued efforts will improve the understanding of the thermoelectric properties of microporous solids.

## EXPERIMENTAL PROCEDURES

### Materials

$NiCl_2 \cdot 6H_2O$ (Fisher Scientific), aqueous ammonia (VWR), ethanol (VWR), isopropanol (VWR), acetone (Sigma-Aldrich), gold wires (25 μm diameter; Alfa Aesar), and carbon paste (graphite conductive adhesive 112; Electron Microscopy Sciences) were purchased from commercial sources and were used without purification.

2,3,6,7,10,11-Hexaaminotriphenylene hexahydrochloride, HATP·6HCl, was synthesized according to a literature procedure.[47]

### Characterization of the Powder of $Ni_3(HITP)_2$

$Ni_3(HITP)_2$ was synthesized by modifying a published procedure, which generates a material exhibiting a higher degree of crystallinity.[24] A quantity of 95.7 mg of $NiCl_2 \cdot 6H_2O$ and 141.9 mg of HATP·6HCl were dissolved in 60 mL of deionized (DI) water in a 250-mL round-bottom flask. The resulting yellow solution was heated to 65°C in an oil bath and treated with 1.5 mL of concentrated aqueous ammonia. The reaction mixture was kept at 65°C for 45 min under continuous air bubbling, upon which the reaction was switched to an inert atmosphere and kept at 65°C for an additional 2 hr. The resulting crude black precipitate was separated from the reaction mixture by centrifugation, soaked in deionized water at room temperature, and washed with water, ethanol, and acetone. Finally the solid product was dried under a stream of nitrogen gas for 12 hr. The product was kept in a nitrogen-filled glovebox. We found that soaking $Ni_3(HITP)_2$ in water under air at elevated temperature for a few hours or exposing it to air for several months significantly reduced its electrical conductivity.

Elemental analysis was performed by Complete Analysis Laboratories (Parsipanny, NJ, USA). C, H, N, and Cl elemental analysis for $Ni_3(C_{18}H_{12}N_6)_{1.8}Cl_{0.6} \cdot 2(C_3H_6O) \cdot 4(H_2O)$ calcd.: C, 48.66%; H, 4.42%; N, 15.96%; Cl, 2.25%; found: C, 48.98%; H, 4.26%; N, 16.21%; Cl, 2.4%.

PXRD patterns were recorded with a Bruker D8 Advance diffractometer equipped with a $\theta/2\theta$ Bragg-Brentano geometry and nickel-filtered Cu K$\alpha$ radiation ($K\alpha_1$ = 1.5406 Å, $K\alpha_2$ = 1.5444 Å, $K\alpha_1/K\alpha_2$ = 0.5). The tube voltage and current were 40 kV and 40 mA, respectively. Samples were prepared by placing thin layers of materials on a zero-background silicon crystal plate. The background was corrected by using the Bruker Diffrac.Suite EVA software.

A Micromeritics ASAP 2020 surface area and porosity analyzer was used to measure $N_2$ adsorption isotherms. An oven-dried sample tube equipped with a TranSeal (Micromeritics) was evacuated and tared. The $Ni_3(HITP)_2$ sample was transferred to the sample tube, which was then capped by a TranSeal. The sample was heated to 80°C and held at this temperature for 26 hr. The evacuated sample tube was weighed and the sample mass was determined by subtracting the mass of the previously tared tube. An $N_2$ adsorption isotherm was measured using a liquid nitrogen bath (77 K). Ultrahigh-purity grade (99.999% purity) $N_2$ and He, oil-free valves, and gas regulators were used for all free space corrections and measurements.

TEM was performed using a Titan 80/300 environmental transmission electron microscope at the Center for Functional Nanomaterials, Brookhaven National Laboratory (Upton, NY, USA). The instrument is equipped with a post-specimen spherical aberration corrector, which was tuned to a flat phase field of 20 mrad. Images were acquired using a Gatan K2-IS direct electron detector, in the Summit mode. Each image was acquired at an electron dose of 30–40 electrons per $Å^2$, as measured by the K2 detector. Images given comprise the sum of up to 20 individual images acquired at 0.2 s per image, using the built-in drift correction in the Gatan software. The summation of shorter image acquisitions allowed us to determine whether the threshold dose for sample damage had been reached, and the summation was truncated at a point before damage was evident. The instrument was operated at 300 kV,

as experiments showed that damage accumulation rates were substantially more rapid at 80 kV, even at the same electron dose.

### Characterization of Pressed Pellets of $Ni_3(HITP)_2$

Pressed pellets of $Ni_3(HITP)_2$ were prepared by placing powders of $Ni_3(HITP)_2$ into a 6-mm inner-diameter trapezoidal split sleeve pressing die (Across International) and pressing the die set by a hydraulic press (MTI) with 3 tons of applied mass for 15 min. The applied pressure was approximately 1 GPa. The thickness of the pellet was measured by a micrometer (Mitutoyo) and varied between 300 μm and 2 mm. The pellet density was approximately 1 $g \cdot cm^{-3}$.

Scanning electron microscopy was conducted at the Harvard Center for Nanoscale Systems (Cambridge, MA, USA) on a Zeiss Ultra55 or a Zeiss Supra55VP field emission scanning electron microscope with an InLens detector and a beam voltage of 3 kV.

Electrical conductivity of pellets of $Ni_3(HITP)_2$ was measured by the van der Pauw method at 25°C, 30°C, 35°C, 40°C, and 45°C. A pellet was placed onto a Si wafer coated with 300 nm of $SiO_2$. Four gold wires were pasted onto the periphery of the pellet by carbon paste in a square configuration. The bare ends of these gold wires were pasted onto the $SiO_2$/Si wafer by carbon paste. The van der Pauw device was mounted onto the sample chuck of a 4-arm probe station (Janis Cryogenics ST-500) with a layer of thermal paste (DuPont Krytox) to enable efficient heat transfer between the device and the sample chuck. Electrical contacts were made by touching carbon paste on the $SiO_2$/Si wafer with gold-plated tungsten probes, whose positions were controlled by micromanipulators. The probe station chamber was evacuated to a pressure of $10^{-5}$ torr. The $Ni_3(HITP)_2$ pellet was heated at 150°C for 2 hr for complete desolvation. It was then cooled down to 25°C and kept in the dark and under dynamic vacuum ($10^{-5}$ torr). The temperature of the pellet was balanced by a heater of the probe station chuck and liquid nitrogen, and was controlled by a temperature controller (Scientific Instrument model 9700). Electrical data were obtained with a Keithley 2450 sourcemeter. The sheet electrical conductance was extracted by the van der Pauw equation. The electrical conductivity was calculated by dividing the sheet electrical conductance by the thickness of the pellet. The error was estimated by considering the error of both sheet electrical conductance and thickness measurements.

The Seebeck coefficient and the thermal conductivity of the pellet were measured using a home-built steady-state measurement system. The pellet (diameter, 6 mm; thickness, 1.8 mm) was sandwiched between a hot junction heater assembly and a cold junction electrode. Silver paste was used to mount the sample to minimize the electrical and thermal contact resistance. The heater assembly consists of a thin film resistance temperature detector as the electrical heater, which was brazed into a small copper block of approximately the same cross-sectional shape and size as the sample. Also embedded in the hot junction assembly are the current and voltage wire leads and a K-type thermocouple. The cold junction consists of a temperature-controllable cold stage, made with a copper heat spreader on top of a thermoelectric cooler module. The whole assembly was contained in a copper radiation shield to minimize radiative heat loss. The $Ni_3(HITP)_2$ pellet was heated at 150°C in vacuum for 2 hr for complete desolvation. The measurement was carried out in a vacuum chamber at a pressure below $10^{-4}$ mbar. After the electrical heater in the hot junction assembly was turned on, the whole system was allowed to reach a thermal steady state. The temperature difference and the generated thermal voltage were recorded at multiple values of input heater power, and the thermal conductivity and Seebeck coefficient were extracted as the slopes of power-versus-temperature

and voltage-versus-temperature curves. The reported values are averages of multiple sweeps of the input heater power, and the error bars represent SDs.

## SUPPLEMENTAL INFORMATION

Supplemental Information includes five figures and one table and can be found with this article online at http://dx.doi.org/10.1016/j.joule.2017.07.018.

## AUTHOR CONTRIBUTIONS

L.S., B.L., M.D.A., G.C., F.L., and M.D. designed and initiated the research. L.S. and D.S. synthesized and characterized the powder of $Ni_3(HITP)_2$, made pressed pellets, and performed scanning electron microscopy and electrical conductivity measurements. B.L., D.K., and J.Z. performed steady-state thermal conductivity and Seebeck coefficient measurements. L.S., E.A.S., and D.Z. performed TEM imaging. V.S. and A.A.T. helped synthesize $Ni_3(HITP)_2$. Y.G. performed surface area measurements. L.S., F.L., and M.D. analyzed data. All authors participated in the discussion. L.S. drafted the manuscript, and F.L. and M.D. revised it. All authors commented on the manuscript.

## ACKNOWLEDGMENTS

Work at MIT was supported as part of the Center for Excitonics, an Energy Frontier Research Center funded by the U.S. DOE-BES under award no. DE-SC0001088 (MIT). Work at Sandia National Laboratories was supported by the Sandia Laboratory Directed Research and Development (LDRD) Program. Sandia National Laboratories is a multimission laboratory managed and operated by National Technology and Engineering Solutions of Sandia, a wholly owned subsidiary of Honeywell International, for the US Department of Energy's National Nuclear Security Administration under contract DE-NA-0003525. Part of this work was performed in part at Harvard University at the Center for Nanoscale Systems (CNS), a member of the National Nanotechnology Coordinated Infrastructure Network (NNCI), which is supported by the National Science Foundation under award no. 1541959. This work used resources of the Center for Functional Nanomaterials, which is a US DOE Office of Science User Facility, at Brookhaven National Laboratory under contract number DE-SC0012704. We thank E.M. Miner, Dr. M.G. Campbell, and Dr. A.M. Schimpf for helpful discussions about sample preparation, Dr. X. Huang for assistance with preliminary thermal conductivity measurements, Dr. X. Zhang for assistance with preliminary electrical conductivity measurements, and G. Skorupskii, T. Soejima, Dr. D. Nykypanchuk, and Dr. A. Akey for helpful discussions about sample characterization.

Received: May 24, 2017
Revised: July 8, 2017
Accepted: July 31, 2017
Published: September 6, 2017

## REFERENCES

1. Goldsmid, H.J. (2016). In Introduction to Thermoelectricity (Heidelberg, Germanay: Springer), pp. 9–24.

2. Minnich, A.J., Dresselhaus, M.S., Ren, Z.F., and Chen, G. (2009). Bulk nanostructured thermoelectric materials: current research and future prospects. Energy Environ. Sci. *2*, 466–479.

3. Liu, W., Yan, X., Chen, G., and Ren, Z. (2012). Recent advances in thermoelectric nanocomposites. Nano Energy *1*, 42–56.

4. Liao, B., and Chen, G. (2015). Nanocomposites for thermoelectrics and thermal engineering. MRS Bull. *40*, 746–752.

5. Zhang, Q., Sun, Y., Xu, W., and Zhu, D. (2014). Organic thermoelectric materials: emerging green energy materials converting heat to electricity directly and efficiently. Adv. Mater. *26*, 6829–6851.

6. Lee, H., Vashaee, D., Wang, D.Z., Dresselhaus, M.S., Ren, Z.F., and Chen, G. (2010). Effects of nanoscale porosity on thermoelectric properties of SiGe. J. Appl. Phys. *107*, 094308.

7. Sun, L., Campbell, M.G., and Dincă, M. (2016). Electrically conductive porous metal-organic frameworks. Angew. Chem. Int. Ed. *55*, 3566–3579.

8. Zhang, Y., Day, T., Snedaker, M.L., Wang, H., Krämer, S., Birkel, C.S., Ji, X., Liu, D., Snyder, G.J., and Stucky, G.D. (2012). A mesoporous anisotropic n-Type $Bi_2Te_3$ monolith with low thermal conductivity as an efficient

thermoelectric material. Adv. Mater. *24*, 5065–5070.

9. Xu, B., Feng, T., Agne, M.T., Zhou, L., Ruan, X., Snyder, G.J., and Wu, Y. (2017). Highly porous thermoelectric nanocomposites with low thermal conductivity and high figure of merit from large-scale solution-synthesized $Bi_2Te_{2.5}Se_{0.5}$ hollow nanostructures. Angew. Chem. Int. Ed. *56*, 3546–3551.

10. Zhou, H., Long, J.R., and Yaghi, O.M. (2012). Introduction to metal-organic frameworks. Chem. Rev. *112*, 673–674.

11. Han, L., Budge, M., and Greaney, P.A. (2014). Relationship between thermal conductivity and framework architecture in MOF-5. Comput. Mater. Sci. *94*, 292–297.

12. Huang, B.L., Ni, Z., Millward, A., McGaughey, A.J.H., Uher, C., Kaviany, M., and Yaghi, O.M. (2007). Thermal conductivity of a metal-organic framework (MOF-5): part II. measurement. Int. J. Heat Mass. Transf. *50*, 405–411.

13. Liu, D., Purewal, J.J., Yang, J., Sudik, A., Maurer, S., Mueller, U., Ni, J., and Siegel, D.J. (2012). MOF-5 composites exhibiting improved thermal conductivity. Int. J. Hydrogen Energy *37*, 6109–6117.

14. Purewal, J.J., Liu, D., Yang, J., Sudik, A., Siegel, D.J., Maurer, S., and Müller, U. (2012). Increased volumetric hydrogen uptake of MOF-5 by powder densification. Int. J. Hydrogen Energy *37*, 2723–2727.

15. Jeremias, F., Fröhlich, D., Janiak, C., and Henninger, S.K. (2014). Advancement of sorption-based heat transformation by a metal coating of highly-stable, hydrophilic aluminium fumarate MOF. RSC Adv. *4*, 24073–24082.

16. Schlemminger, C., Næss, E., and Bünger, U. (2015). Adsorption hydrogen storage at cryogenic temperature—material properties and hydrogen ortho-para conversion matters. Int. J. Hydrogen Energy *40*, 6606–6625.

17. Nandasiri, M.I., Liu, J., McGrail, B.P., Jenks, J., Schaef, H.T., Shutthanandan, V., Nie, Z., Martin, P.F., and Nune, S.K. (2016). Increased thermal conductivity in metal-organic heat carrier nanofluids. Sci. Rep. *6*, 27805.

18. Erickson, K.J., Léonard, F., Stavila, V., Foster, M.E., Spataru, C.D., Jones, R.E., Foley, B.M., Hopkins, P.E., Allendorf, M.D., and Talin, A.A. (2015). Thin film thermoelectric metal-organic framework with high Seebeck coefficient and low thermal conductivity. Adv. Mater. *27*, 3453–3459.

19. Stassen, I., Burtch, N., Talin, A., Falcaro, P., Allendorf, M., and Ameloot, R. (2017). An updated roadmap for the integration of metal-organic frameworks with electronic devices and chemical sensors. Chem. Soc. Rev. *46*, 3185–3241.

20. Talin, A.A., Centrone, A., Ford, A.C., Foster, M.E., Stavila, V., Haney, P., Kinney, R.A., Szalai, V., El Gabaly, F., Yoon, H.P., et al. (2013). Tunable electrical conductivity in metal-organic framework thin film devices. Science *343*, 66–69.

21. Park, S.S., Hontz, E.R., Sun, L., Hendon, C.H., Walsh, A., Van Voorhis, T., and Dincă, M. (2015). Cation-dependent intrinsic electrical conductivity in isostructural tetrathiafulvalene-based microporous metal-organic frameworks. J. Am. Chem. Soc. *137*, 1774–1777.

22. Sun, L., Hendon, C.H., Minier, M.A., Walsh, A., and Dincă, M. (2015). Million-fold electrical conductivity enhancement in $Fe_2$(DEBDC) versus $Mn_2$(DEBDC) (E=S, O). J. Am. Chem. Soc. *137*, 6164–6167.

23. Sun, L., Hendon, C.H., Park, S.S., Tulchinsky, Y., Wan, R., Wang, F., Walsh, A., and Dincă, M. (2017). Is iron unique in promoting electrical conductivity in MOFs? Chem. Sci. *8*, 4450–4457.

24. Sheberla, D., Sun, L., Blood-Forsythe, M.A., Er, S., Wade, C.R., Brozek, C.K., Aspuru-Guzik, A., and Dincă, M. (2014). High electrical conductivity in $Ni_3$(2,3,6,7,10,11-hexaiminotriphenylene)$_2$, a semiconducting metal-organic graphene analogue. J. Am. Chem. Soc. *136*, 8859–8862.

25. Kambe, T., Sakamoto, R., Hoshiko, K., Takada, K., Miyachi, M., Ryu, J.-H., Sasaki, S., Kim, J., Nakazato, K., Takata, M., et al. (2013). π-Conjugated nickel bis(dithiolene) complex nanosheet. J. Am. Chem. Soc. *135*, 2462–2465.

26. Kambe, T., Sakamoto, R., Kusamoto, T., Pal, T., Fukui, N., Hoshiko, K., Shimojima, T., Wang, Z., Hirahara, T., Ishizaka, K., et al. (2014). Redox control and high conductivity of nickel bis(dithiolene) complex π-nanosheet: a potential organic two-dimensional topological insulator. J. Am. Chem. Soc. *136*, 14357–14360.

27. Huang, X., Sheng, P., Tu, Z., Zhang, F., Wang, J., Geng, H., Zou, Y., Di, C.-A., Yi, Y., Sun, Y., et al. (2015). A two-dimensional π-d conjugated coordination polymer with extremely high electrical conductivity and ambipolar transport behaviour. Nat. Commun. *6*, 7408.

28. Miner, E.M., Fukushima, T., Sheberla, D., Sun, L., Surendranath, Y., and Dincă, M. (2016). Electrochemical oxygen reduction catalysed by $Ni_3$(hexaiminotriphenylene)$_2$. Nat. Commun. *7*, 10942.

29. Sheberla, D., Bachman, J.C., Elias, J.S., Sun, C.-J., Shao-Horn, Y., and Dincă, M. (2017). Conductive MOF electrodes for stable supercapacitors with high areal capacitance. Nat. Mater. *16*, 220–224.

30. Wu, G., Huang, J., Zang, Y., He, J., and Xu, G. (2016). Porous field-effect transistors based on a semiconductive metal-organic framework. J. Am. Chem. Soc. *139*, 1360–1363.

31. Stock, N., and Biswas, S. (2012). Synthesis of metal-organic frameworks (MOFs): routes to various MOF topologies, morphologies, and composites. Chem. Rev. *112*, 933–969.

32. Houk, R.J.T., Jacobs, B.W., El Gabaly, F., Chang, N.N., Talin, A.A., Graham, D.D., House, S.D., Robertson, I.M., and Allendorf, M.D. (2009). Silver cluster formation, dynamics, and chemistry in metal-organic frameworks. Nano Lett. *9*, 3413–3418.

33. Jacobs, B.W., Houk, R.J.T., Anstey, M.R., House, S.D., Robertson, I.M., Talin, A.A., and Allendorf, M.D. (2011). Ordered metal nanostructure self-assembly using metal-organic frameworks as templates. Chem. Sci. *2*, 411–416.

34. Zhu, Y., Ciston, J., Zheng, B., Miao, X., Czarnik, C., Pan, Y., Sougrat, R., Lai, Z., Hsiung, C.-E., Yao, K., et al. (2017). Unravelling surface and interfacial structures of a metal-organic framework by transmission electron microscopy. Nat. Mater. *16*, 532–536.

35. van der Pauw, L.J. (1958). A method of measuring specific resistivity and Hall effect of discs of arbitrary shape. Philips Res. Rep. *13*, 1–9.

36. van der Pauw, L.J. (1958). A method of measuring the resistivity and Hall coefficient on lamellae of arbitrary shape. Philips Tech. Rev. *20*, 220–224.

37. Kraemer, D., Sui, J., McEnaney, K., Zhao, H., Jie, Q., Ren, Z.F., and Chen, G. (2015). High thermoelectric conversion efficiency of MgAgSb-based material with hot-pressed contacts. Energy Environ. Sci. *8*, 1299–1308.

38. Kraemer, D., and Chen, G. (2014). High-accuracy direct ZT and intrinsic properties measurement of thermoelectric couple devices. Rev. Sci. Instrum. *85*, 045107.

39. Kraemer, D., and Chen, G. (2014). A simple differential steady-state method to measure the thermal conductivity of solid bulk materials with high accuracy. Rev. Sci. Instrum. *85*, 025108.

40. Bubnova, O., and Crispin, X. (2012). Towards polymer-based organic thermoelectric generators. Energy Environ. Sci. *5*, 9345–9362.

41. Poudel, B., Hao, Q., Ma, Y., Lan, Y., Minnich, A., Yu, B., Yan, X., Wang, D., Muto, A., Vashaee, D., et al. (2008). High thermoelectric performance of nanostructured bismuth antimony telluride bulk alloys. Science *320*, 634–638.

42. Zhao, L.-D., Lo, S.-H., Zhang, Y., Sun, H., Tan, G., Uher, C., Wolverton, C., Dravid, V.P., and Kanatzidis, M.G. (2014). Ultralow thermal conductivity and high thermoelectric figure of merit in SnSe crystals. Nature *508*, 373–377.

43. Grosso, G., and Parravicini, G.P. (2014). In Solid State Physics (Amsterdam, Netherland: Academic Press), pp. 483–528.

44. Snyder, G.J., and Toberer, E.S. (2008). Complex thermoelectric materials. Nat. Mater. *7*, 105–114.

45. Sootsman, J.R., Chung, D.Y., and Kanatzidis, M.G. (2009). New and old concepts in thermoelectric materials. Angew. Chem. Int. Ed. *48*, 8616–8639.

46. Chen, S., Dai, J., and Zeng, X.C. (2015). Metal-organic kagome lattices $M_3$(2,3,6,7,10,11-hexaiminotriphenylene)$_2$ (M = Ni and Cu): from semiconducting to metallic by metal substitution. Phys. Chem. Chem. Phys. *17*, 5954–5958.

47. Chen, L., Kim, J., Ishizuka, T., Honsho, Y., Saeki, A., Seki, S., Ihee, H., and Jiang, D. (2009). Noncovalently netted, photoconductive sheets with extremely high carrier mobility and conduction anisotropy from triphenylene-fused metal trigon conjugates. J. Am. Chem. Soc. *131*, 7287–7292.